Earthquake Engineering, Tenth World Conference © 1994 Balkema, Rotterdam. ISBN 90 5410 060 5

Nonlinear time history analysis of R/C frame-wall buildings to determine the ductility demand of gravity load columns

Hugo Bachmann, Thomas Wenk & Peter Linde
Swiss Federal Institute of Technology (ETH), Zürich, Switzerland

ABSTRACT: A dynamic nonlinear analysis method for R/C buildings subjected to earthquake action is presented. Nonlinear elements for the modelling of plastic hinges in walls, beams and columns are explained. In numerical examples, a capacity designed frame-wall building subjected to different ground motions is analysed, and an evaluation of the ductility demand of the plastic hinges in walls, beams, and especially in the slender gravity load columns is made. The structural behaviour was governed by the wall and the gravity load column ductility demand remained in acceptable limits.

INTRODUCTION

The design of multi storey reinforced concrete buildings for earthquake action may be efficiently accomplished with the capacity design method (Paulay, Bachmann, and Moser, 1990) and (Paulay and Priestley, 1992). Briefly explained, this method focuses on the establishment of clearly defined plastic hinge zones, the proper detailing of these, and the protection of the remaining elastic parts of the building against yielding. For the verification of the structural behaviour during an earthquake, there exists however a need for a nonlinear dynamic analysis method, as well as for design aid for eccentric and complicated building configurations.

For the modelling of the plastic hinge zones, nonlinear elements were developed, and implemented as user defined elements into an existing general finite element code (Abaqus, 1991). These elements, treating the behaviour of plastic hinge zones in structural walls, beams, and columns are presented and used in this paper.

A reinforced concrete frame-wall building will serve as numerical example, designed by the equivalent lateral static force method for two different levels of global displacement ductility. The columns are designed as relatively slender gravity load columns, and the structural wall is assigned to resist all earthquake action. This design is commonly found in Switzerland and allows a clear design procedure, and a clear flow of design forces.

In this study, a relatively stiff structural wall is combined with seismically weak gravity load columns. This study may be seen as an addition to studies presented recently (Bachmann, Wenk, and Linde, 1991) on a relatively flexible structural wall combined with a moment resisting frame, where the strong column-weak beam concept was respected.

MODELLING OF STRUCTURAL WALLS

In this paper, the numerical modelling of structural walls is carried out with a macro model, consisting of four non-linear springs connected by rigid beams, as seen in figure 1. The outer vertical springs model the flexural behaviour of the entire wall cross section, and follow hysteretic rules seen in figure 2, showing spring force vs. spring displacement.

The main features of the hysteretic rules consist of the skeleton curve, and of unloading curves. The skeleton curve is made up of an elastic compressive stiffness K_{el}, a cracked tensile stiffness K_{cr} and a yielding stiffness K_y, the latter two of which are taken as fractions of the compressive elastic stiffness. The cracked tensile stiffness may be found in the range of 40% to 90% of the elastic stiffness. In this study it was set to 70%. The yield stiffness may vary from below 1% up to about 3%, much depending on how large ductilities are to be modelled. In this study the yield stiffness was set to 2% of the elastic stiffness.

The unloading rule in the tensile region as well as the reloading rule in the compressive region of figure 2, are both parallel to the stiffness K_u seen in the figure. The reloading in the tensile region occurs towards the maximum reached displacement. The unloading in the compressive region occurs towards a point $\alpha_{cl}F_y$ on the elastic compressive branch, denoting the point where flexural cracks are closing. This point determines the fatness of the hysteresis loops, and its force level was found to be roughly equal to the effective axial force acting on the wall section, in order to get reasonable flexural hysteretic behaviour. A more detailed discussion on the hysteretic rules, is provided in (Linde, 1992).

The central vertical spring models the axial behaviour together with the flexural springs, and is active only in compression. The horizontal spring models the shear

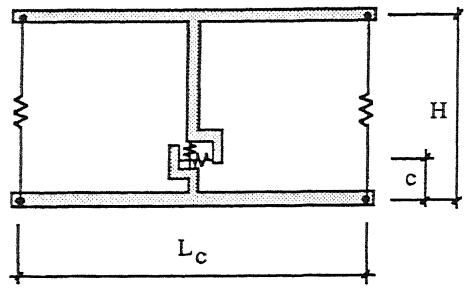

Figure 1. Macro model for structural wall

behaviour, and is located at a distance c the from the bottom of the model, where $0 < c < H$. A bilinear origin oriented hysteretic model was considered sufficient for the shear behaviour in this paper, modelling elastic and cracked stiffness only. The location of the horizontal spring may be seen as an evaluation point of the macro element for the bending moment distributed along the height of the element, and secondly as a kinematic centre of rotation. Concerning the bending moment it would be desirable to set the evaluation point somewhere in the lower third of the height, due to the mostly trapezoidal form of the moment distribution along the height, although a quite uniform moment may occur over the height due to higher modes in dynamic analyses. Concerning the kinematics, elastic theory and uniform bending moment over the element height only, would imply that c be equal to 0.5H, however, nonlinear behaviour suggests a lower value. In this report, c was taken as 0.25H, a value which has proved to give reasonable agreement with experimental data, in combination with discretisation of the plastic hinge zone into several elements.

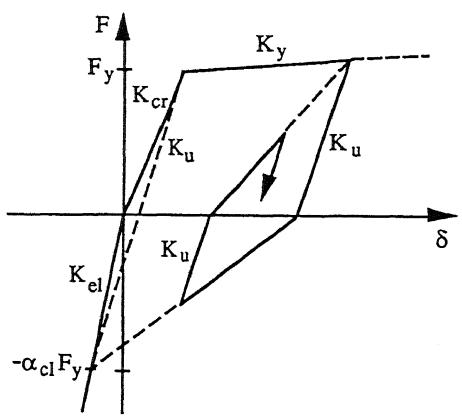

Figure 2. Hysteretic rules of wall flexural springs

MODELLING OF FRAMES

Nonlinear elements were employed for the modelling of the plastic hinges in beams and columns. The length of these elements is taken as the T-beam height or the column width, respectively. The evaluation of the bending moment is performed at mid-length of the elements. The hysteretic rules consist of a modified Takeda model, see figure 3, which displays the moment vs. curvature relations.

For the beams, different positive and negative yield moments are employed, which is of importance when gravity loads are considerable. To account for concrete cracking, the elastic flexural stiffness of the beams, seen in the figure as EI_{el}, is taken as 40% of the uncracked section's flexural stiffness.

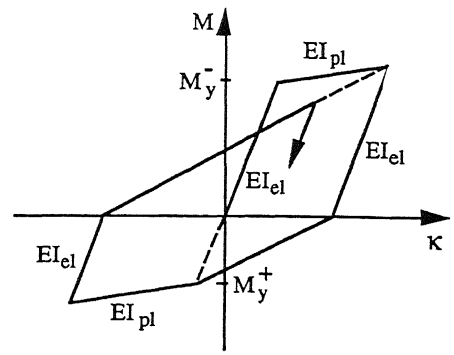

Figure 3. Hysteretic rules for beam and column plastic hinge elements

For the column plastic hinge elements, the axial force is taken into account by the use of an idealised moment-axial force interaction diagram, which is seen in figure 4. The yield moment M_y of the column skeleton curve is thus adjusted according to the instantaneous axial force. The elastic flexural stiffness of the columns is taken as 80% of the uncracked section's flexural stiffness.

For the nonlinear elements in beams and columns the yield stiffness, EI_{pl}, is taken as a fraction of 2% of the elastic stiffness. Further details on the modelling of frame elements are given in (Wenk, 1992).

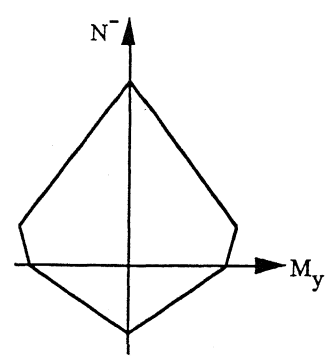

Figure 4. Moment-normal force relation for column plastic hinge elements

FRAME-WALL BUILDING STRUCTURE

For the numerical studies in this paper, an eight storey reinforced concrete frame-wall building structure is used. The structure type considered consists of: two structural walls over the whole building height, floor slabs with beams running in one direction, and reinforced concrete gravity load columns built-in at the floors. The structural walls are mainly subjected to horizontal wind and earthquake actions while the slender columns are designed for gravity loads only.

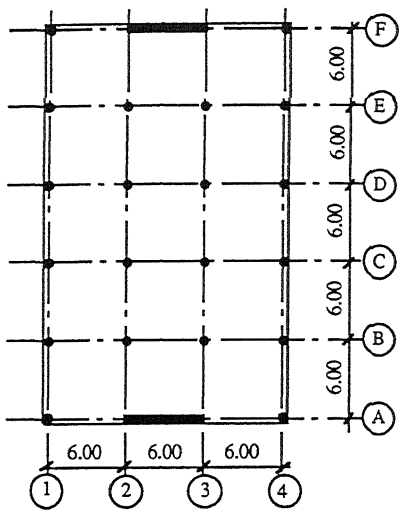

Figure 5. Plan of eight storey frame-wall building

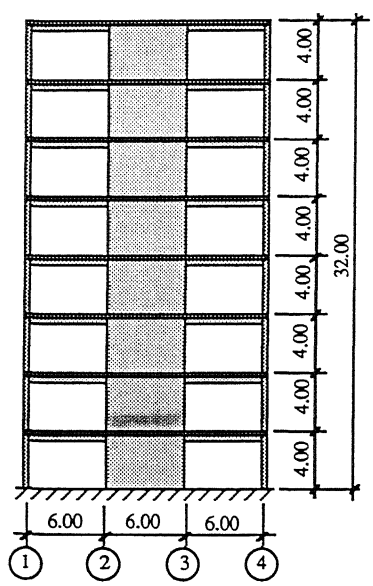

Figure 6. Elevation of eight storey frame-wall building

This structure type is very common in Switzerland and offers the following advantages: clear and transparent flow of forces, ease of construction, and standardisation of details. Elevation and plan is shown in figures 5 and 6, respectively.

For the design of the building structure, the capacity design method was used, employing an equivalent static force, based on an elastic design spectrum and with force reduction according to two different ductility levels, (Paulay, Bachmann, and Moser, 1990). The used design spectrum assumes the seismic zone 3b, and mid-stiff soil, of the Swiss Standard (SIA Standard 160, 1991). The overstrength of the structure was considered by reducing the equivalent static force by an overstrength reduction factor C_d equal to 0.65 according to the Swiss Standard SIA 160.

Two different global displacement ductility levels were chosen. The first of these two, referred to as the limited ductility level, employed a global displacement ductility factor μ_Δ equal to three. The second ductility level, known as the full ductility level, used a μ_Δ equal to five. In the Swiss Standard SIA 160 the ductility factor is designated K. For both designs, the structural wall is assigned to resist all earthquake action.

The material was specified according to the SIA Standard 162 as follows. Reinforcing steel: S500 (design strength: f_y = 460 MPa); Walls and beams: concrete class B40/30 (design strength: f_c = 19.5 MPa), columns: concrete class B65/55 (design strength: f_c = 36 MPa). To realistically account for overstrength, the design strengths of the reinforcing steel and of the wall concrete were modified to nominal values for the time integration analysis as follows: f_y = 550 MPa, f_c=30 MPa (wall only).

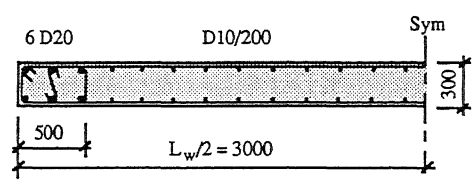

Figure 7. First storey cross section of wall designed for limited ductility level of $\mu_\Delta = 3$

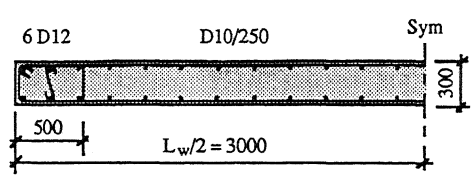

Figure 8. First storey cross section of wall designed for full ductility level of $\mu_\Delta = 5$

The design of the structural wall was governed by earthquake as predominant action and live load as accompanying action. For both ductility levels, a rectangular cross section was chosen for the structural wall, 6.0 m in length, and 300 mm thick. In both cases, the out-of-plane buckling problem in the plastic hinge region was considered, and by a recently published method (Paulay and Priestley, 1992) found to be in order. For the full ductility level, the chosen wall thickness barely met the suggested buckling requirement.

The flexural reinforcement at the wall plastic hinge, located at the base of the wall, and extending 6.0 m upwards was designed as follows. For the limited ductility level, the wall obtained vertical reinforcement ratios of 0.26% distributed over the section, except at both ends, where a confined zone of 500 mm length contained 1.2%. The wall designed for full ductility level, obtained 0.21% and 0.5%, for the same areas, respectively. Figures 7 and 8 show the wall cross sections. The horizontal wall reinforcement has a ratio of 0.20% over the first storey.

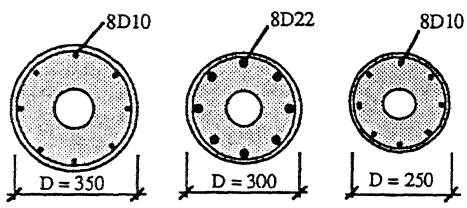

Figure 9. Gravity load column cross sections: Column axis B2, B3,...(left), Column axis B1, B4,... (centre), Column axis A1, A4, F1, and F4 (right)

The gravity load columns were made up of prefabricated spirally confined circular sections. The column diameter is 350 mm for interior columns and 300 mm for exterior columns in axes B to E. For the exterior axes A and F the column diameter is 250 mm. The columns were designed for live load as predominant action. The axial reinforcement ratio was set at 1.4% for interior columns and at 4.8 % for exterior columns.

The slab thickness of 250 mm is constant for all floors, and the T-beams, running parallel to the structural walls, have a width of 400 mm and a height of 500 mm including the slab.

GROUND MOTION

As input for the nonlinear time history analysis, two artificially generated ground acceleration histories were used, and in addition, one recorded ground acceleration. Both generated histories base on elastic design response spectra. The first is the Swiss Standard (SIA 160) design spectrum for zone 3b (highest seismicity) for medium stiff soils, with a max. design ground acceleration of 0.16g and a damping ratio of 5%. The second spectrum is the proposed Eurocode 8 (EC8) design spectrum and for medium stiff soil, scaled to the same maximum ground acceleration of 0.16g and equally a damping ratio of 5%. The plateau amplification factor for the EC8 spectrum is 2.5, compared to 2.12 for the SIA spectrum. Both design spectra are shown in figure 10. It may be noted that for the EC8 spectrum, the corner frequency values of the plateau are moved towards the low frequency side compared to the SIA spectrum. As a result, the spectral values of the EC8 spectrum at the first natural frequency (0.9 Hz for both designs) is roughly 40 % higher than the corresponding SIA value.

The first ground acceleration history, which is based on the SIA spectrum, is shown in figure 11. The duration is 10 s, with a strong motion phase of around 7 s. The second ground acceleration history, based on the EC8 is shown in figure 12. The duration is as well 10 s, also with a strong motion phase of 7 s.

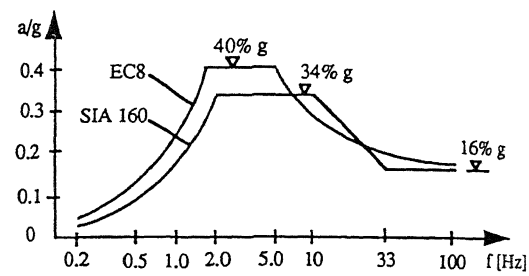

Figure 10. Elastic acceleration design response spectra of SIA 160 zone 3b, and EC8, both for medium stiff soils and 5% damping

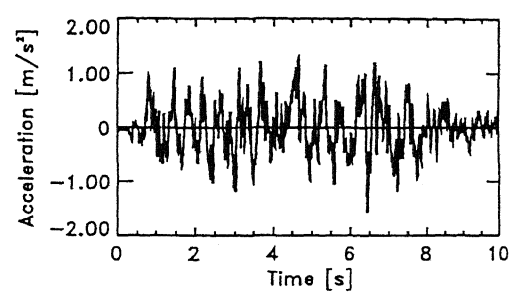

Figure 11. Artificial time history ground acceleration, based on SIA 160

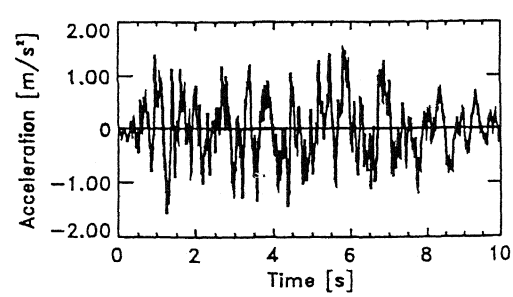

Figure 12. Artificial time history ground acceleration, based on EC8

As recorded ground acceleration, the N-S component recorded at Tolmezzo of the 1976 Friuli earthquake, was used. The record was truncated to obtain the same length as the two generated time histories. The response spectrum for 5% damping is shown in figure 13, and the record in figure 14. The spectral value of the Tolmezzo record at the first natural frequency of the building of 0.9 Hz is about the same as for the EC8, both of which are about 40% higher than the SIA spectral value.

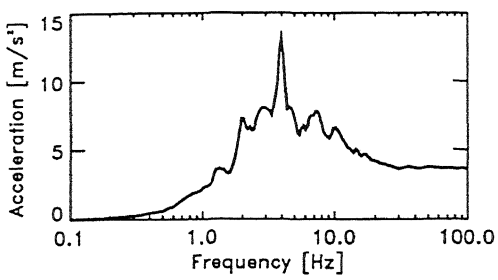

Figure 13. Acceleration response spectrum of the recorded Tolmezzo N-S component, for 5 % damping

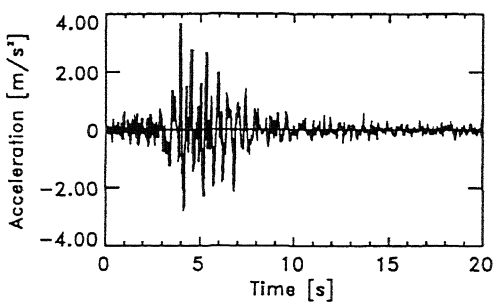

Figure 14. Recorded time history ground acceleration, Tolmezzo N-S component

TIME HISTORY ANALYSIS

The nonlinear elements described in the first sections of this paper, were implemented as user defined elements in an existing general purpose FE code (Abaqus). The previously described eight storey frame-wall building structure was discretised by user defined elements and by linear elastic library elements.

Earthquake action was assumed in the direction of the structural walls, and with a horizontal component only. By use of symmetry, only half the building was analysed, thus including one exterior frame with wall (denoted A in figure 5) and two interior frames (B and C in figure 5). This, combined with assumed moment-weak and in-plane-rigid floor diaphragms, allowed for a two dimensional analysis by coupling the interior frames to the exterior by prescribing same horizontal displacements at every floor level. The two interior frames were lumped into a single frame by doubling the relevant section properties. The discretisation of the analysed frame is shown in figure 15.

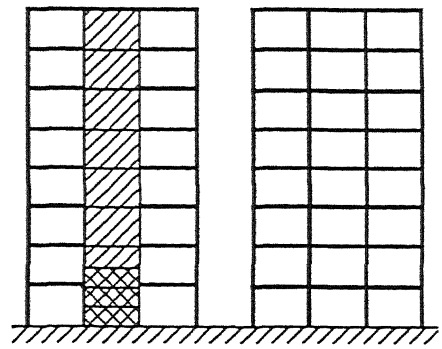

Figure 15. Discretisation of half of symmetric building; frame with wall (left), and interior frames (right), (horizontal floor displacements coupled)

The plastic hinge of the wall, stretching into the second storey, was discretised into three elements of user type. The rest of the second storey, as well as the remaining storeys of the wall was also modelled by user elements to allow for cracking nonlinearity.

The frame was discretised into user elements for the plastic hinges at both ends of the columns and the beams adjacent to the wall, and into linear elastic library beam elements for the rest.

In addition to the hysteretic damping, provided by the nonlinear user elements, a small percentage of Rayleigh damping was utilised to damp higher frequencies. Two percent damping was determined at 0.3 Hz (about one third of first natural frequency, to allow for yielding) and at 5 Hz (second frequency). The Rayleigh damping coefficients were obtained as $\alpha = 0.07$, $\beta = 0.0012$. The resulting additional damping is displayed in figure 16, in which also the first four natural frequencies are indicated.

The storey masses were modelled as lumped library mass elements. The nonlinear time integration analyses, utilising a time increment of 0.01s, were carried out for a duration of 12s, and were preceded by a linear static gravity load step. An incremental-iterative procedure was employed, with residual tolerances set to about 1% of maximum element forces.

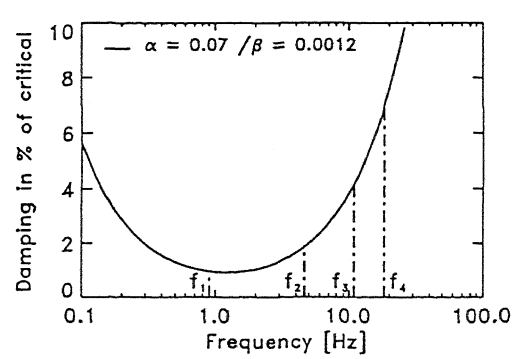

Figure 16. Rayleigh damping for 2% at 0.3 Hz, and 5 Hz, used in addition to hysteretic damping.

Two different structural designs of the eight storey frame-wall building were analysed by a nonlinear time history analysis. The designs were previously dimensioned for the equivalent static force based on the elastic design response spectrum for the seismic zone 3b of the Swiss Standard (SIA Standard 160, 1991) and with force reduction for limited (design $\mu_\Delta = 3$) and full (design $\mu_\Delta = 5$) displacement ductility, respectively. Each of these two designs was then subjected to three different ground motion inputs, giving a total of six nonlinear analyses. These inputs consisted of the earlier discussed two SIA- and EC8-compatible artificial ground acceleration histories, and the third ground motion was made up of the recorded Tolmezzo N-S horizontal component.

DISCUSSION OF RESULTS

Rotational Ductility Demand

Plastic deformation may develop at three general locations; in the plastic hinge zone at the base of the wall, in the plastic hinge zones of the columns, and in the beam plastic hinge zones adjacent to the structural wall.

The distributions of plastic deformation are shown in figures 17 to 22, by small dials indicating the maximum rotational ductility demand (RDD) during the 12 s. time integration analysis. The wall dials indicate the maximum RDD obtained from left and right curvatures, respectively. The RDD of each of the three macro elements forming the plastic hinge is given individually.

The RDD of the gravity load columns is in general highest at the top stories. The lower stories may even remain elastic. The maximum RDD of all gravity load columns are summarised in figure 23. Under the SIA seismic input, a maximum RDD of only about four is reached in the top storey. Considerably higher RDD's are reached for the EC8 (RDD = 7), and in particular for the Tolmezzo seismic input (RDD = 10).

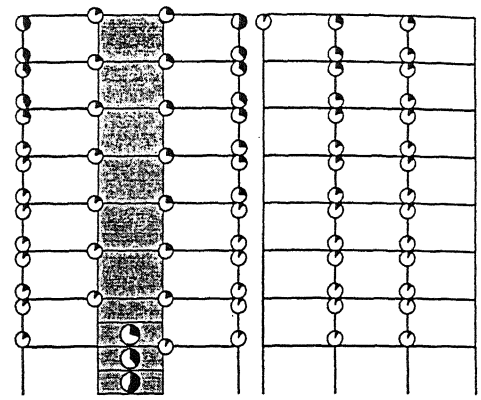

Design K=3, Seismic Input: EC8

RDD: 3.0 6.0 9.0 12.0 Maximum RDD: 6.8

Figure 18. Rotational ductility demands, Design $\mu_\Delta = 3$, seismic input EC8.

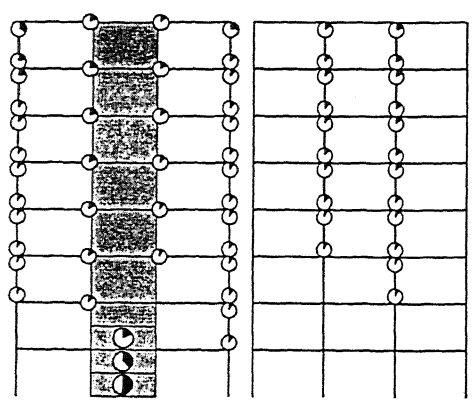

Design K=3, Seismic Input: SIA

RDD: 3.0 6.0 9.0 12.0 Maximum RDD: 6.3

Figure 17. Rotational ductility demands, Design $\mu_\Delta = 3$, seismic input SIA.

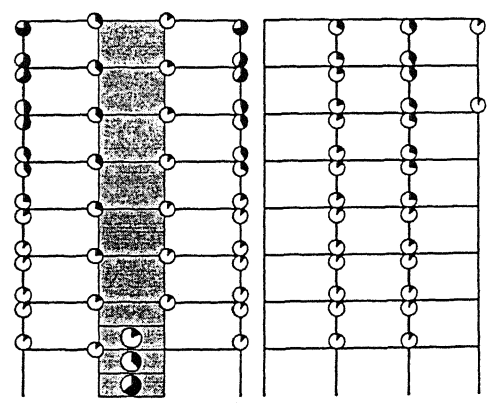

Design K=3, Seismic Input: TOLMEZZO

RDD: 3.0 6.0 9.0 12.0 Maximum RDD: 9.4

Figure 19. Rotational ductility demands, Design $\mu_\Delta = 3$, seismic input Tolmezzo.

It must be remembered that the structure was designed for the earthquake SIA 160, and not for the EC8 and Tolmezzo earthquakes (compare figures 10 and 13). An RDD of four is fairly low, and no special detailing of the column plastic hinge zones is to be considered, whereas for higher RDD's, a special confining reinforcement according to the rules of (Paulay, Bachmann, and Moser, 1990) is necessary. In general the column RDD is higher for the design $\mu_\Delta = 5$ than for the design $\mu_\Delta = 3$, but the difference is small compared to the influence of the seismic input.

A summary of the wall RDD is given in figure 24. In order to show the influence of the nonlinear gravity load columns a reference analysis comprising a nonlinear wall and a frame modelled by linear elements was carried out, for all six design and input combinations. The resulting wall RDD's were displayed by empty circles (wall + linear frame, and by full circles (wall + nonlinear frame) in the figure. The gravity load columns generally have a beneficial (lowering) effect on the maximum RDD of the wall.

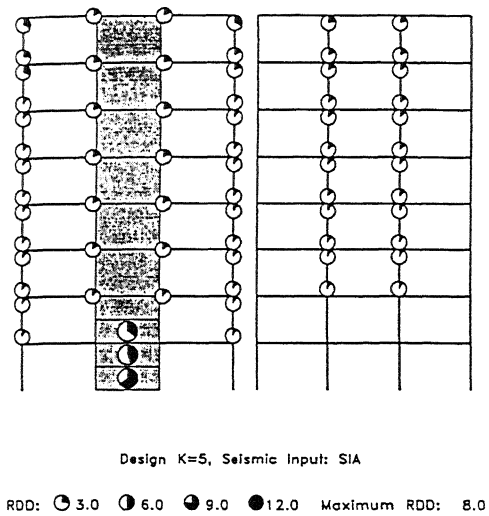

Figure 20. Rotational ductility demands, Design $\mu_\Delta = 5$, seismic input SIA.

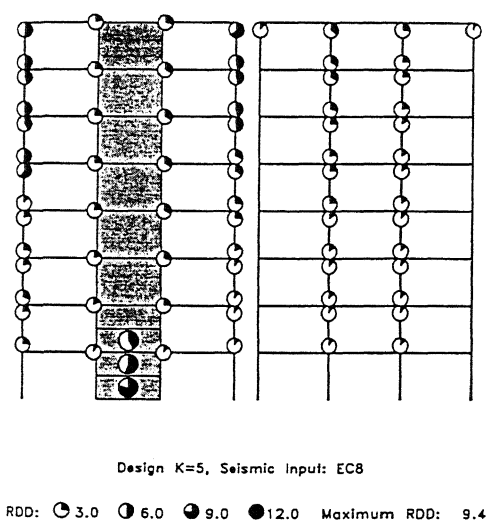

Figure 21. Rotational ductility demands, Design $\mu_\Delta = 5$, seismic input EC8.

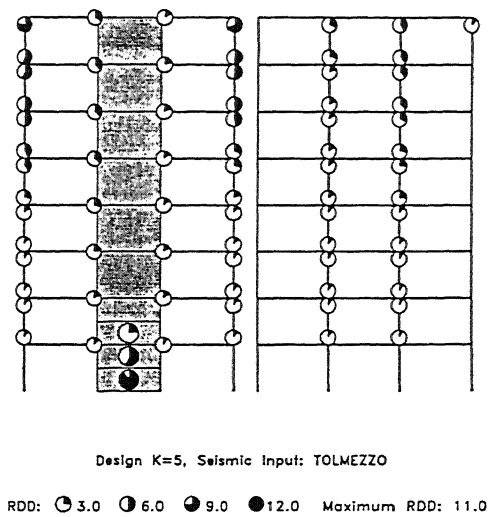

Figure 22. Rotational ductility demands, Design $\mu_\Delta = 5$, seismic input Tolmezzo.

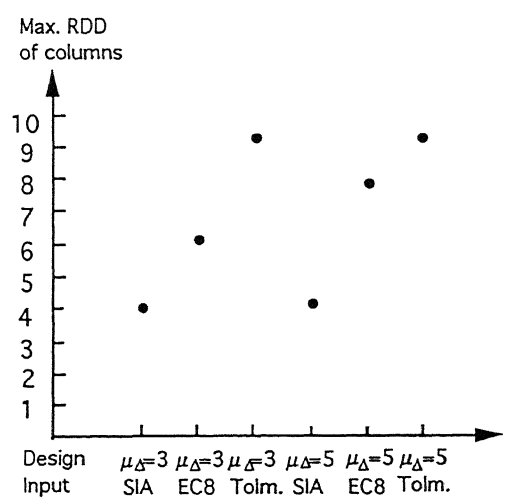

Figure 23. Maximum rotational ductility demands (RDD) of gravity load columns

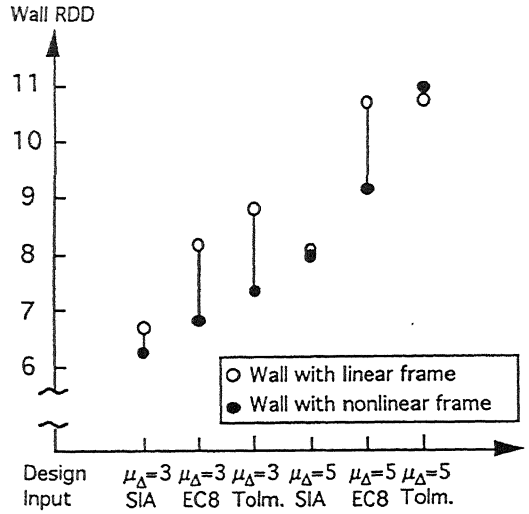

Figure 24. Influence of gravity load columns on rotational ductility demand (RDD) of structural wall.

Horizontal Roof Displacement

The horizontal roof displacements are shown in figures 25 to 27, grouped according to the three seismic inputs. The solid lines indicate the design $\mu_\Delta = 3$, while the dotted lines show design $\mu_\Delta = 5$. The design $\mu_\Delta = 5$ (full ductility) produces only slightly higher roof displacements than the design $\mu_\Delta = 3$ (limited ductility).

For these roof displacement histories, corresponding roof response spectra were computed. These spectra are shown in figures 28 to 30 compared to the ground motion spectra, all for 5% damping. For all cases, sharp peaks are visible just below the second natural frequency of the structure, where peak amplification by a factor of almost four is obtained compared to the ground response spectra.

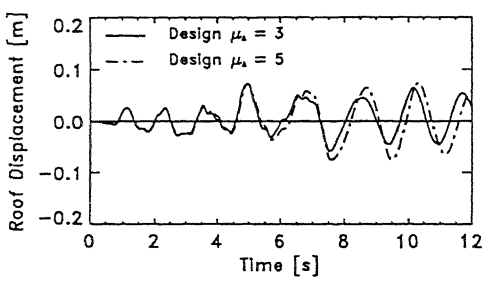

Figure 25. Horizontal roof displacements for seismic input SIA

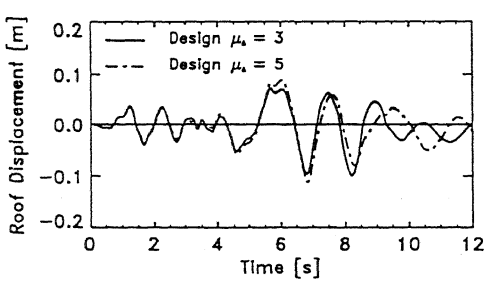

Figure 26. Horizontal roof displacements for seismic input EC8

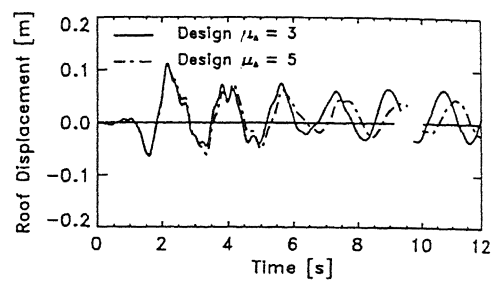

Figure 27. Horizontal roof displacements for seismic input Tolmezzo

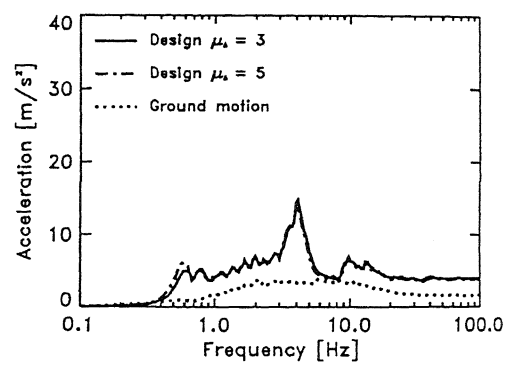

Figure 28. Response spectrum of horizontal roof and ground accelerations, seismic input SIA, for 5% damping

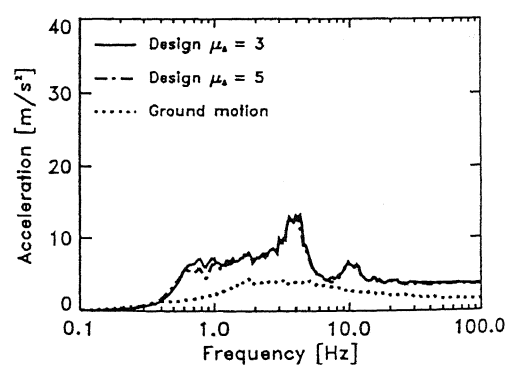

Figure 29. Response spectrum of horizontal roof and ground accelerations, seismic input EC8, for 5% damping

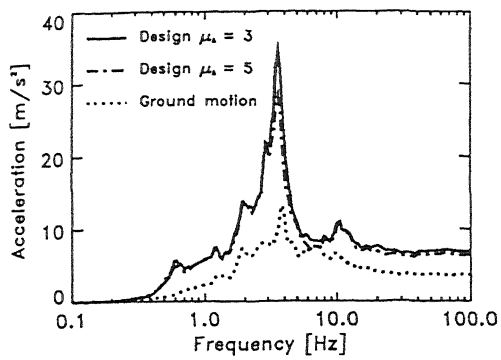

Figure 30. Response spectrum of horizontal roof and ground accelerations, seismic input Tolmezzo, for 5% damping

Interstorey Drift Index

Especially important for the structural detailing of gravity load columns, but also for the design of nonstructural elements, is the interstorey drift. The horizontal displacement difference between two stories, divided by the storey height, is here denoted as interstorey drift index (IDI). The maximum IDI, denoted as IDI_{max}, was extracted during the time integration analysis, and is here displayed in figure 31 on the left for the design $\mu_\Delta = 3$, and for the SIA and EC8 seismic inputs.

In the same figure on the right is shown the highest column rotational ductility demand for each storey, extracted from the same analyses. The maximum RDD are obtained in the top stories, where the IDI equally reaches its maximum. For the upper stories, the IDI remains practically constant, due to linear wall response in this region. Going downwards from the top storey, the column RDD is decreasing sharper than the corresponding IDI, which is largely due to increasing column flexural strength as a result of higher axial load.

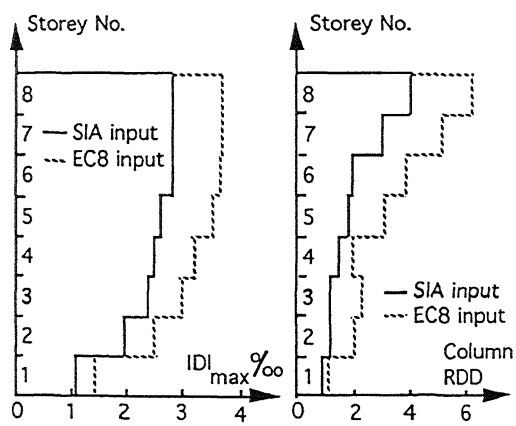

Figure 31. Maximum interstorey drift index (IDI_{max}) (left), and maximum gravity load column rotational ductility demand (RDD) (right), for corresponding stories , both for design $\mu_\Delta = 3$

Moment Curvature Relation

As an example of the nonlinear response of the wall plastic hinge zone, the moment vs. curvature relation of the three macro elements used to discretise this region, are shown in figure 32, for the design $\mu_\Delta = 3$ and seismic input SIA. The lowest plot in figure 32 is displaying the macro element closest to the base which reaches a RDD of 6.3 (compare figure 17). At the upper end of the plastic hinge zone, the maximum RDD has dropped to only 2.1 (top plot in figure 32).

For the design of the gravity load columns, the nonlinear behaviour of the column plastic hinge is of interest. The moment-curvature relation is shown in

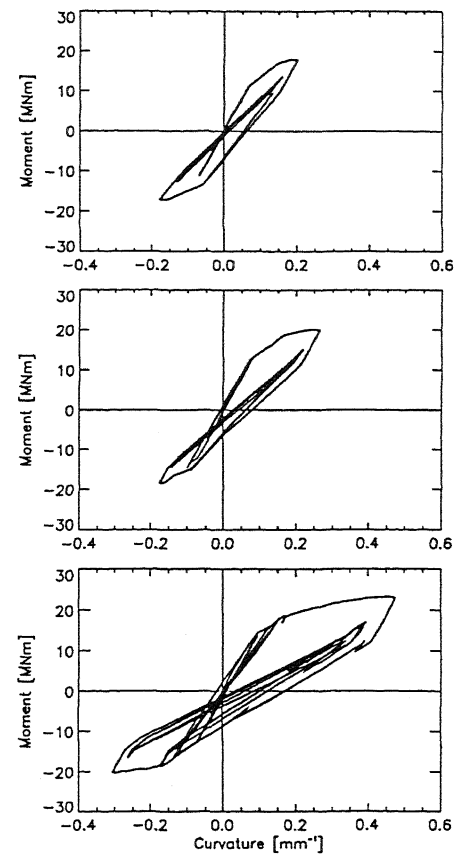

Figure 32. Moment curvature relationship of the three macro elements of the wall plastic hinge, design $\mu_\Delta = 3$, seismic input SIA

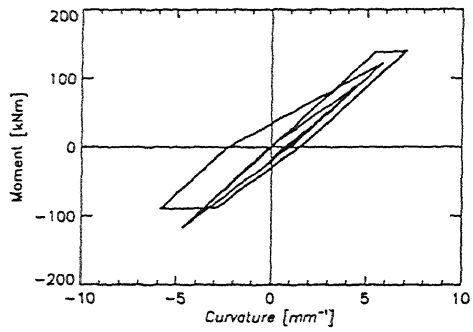

Figure 33. Typical moment curvature relationship of column plastic hinge

figure 33, for an interior column, design $\mu_\Delta = 3$, and seismic input EC8.

SUMMARY AND CONCLUSIONS

In this paper, finite elements developed for simulating the nonlinear behaviour of structural walls, beams and columns during seismic action are presented. These elements were used in the modelling of an eight storey frame-wall building with relatively slender gravity load columns. The building structure was designed according to the Swiss Standard SIA 160, by the equivalent static force method with an overstrength reduction factor of 0.65, and a further force reduction according to two ductility levels, of $\mu_\Delta = 3$ and $\mu_\Delta = 5$, using the capacity design principles. Ground acceleration from different sources used as time history input was described, and a series of nonlinear time integration analyses were performed.

A number of major conclusions could be drawn from the results as follows:

The maximum column RDD is largely determined by the behaviour of the structural wall. For the seismic input SIA, only relatively small RDD's were obtained, even in the case of design μ_Δ=5. Only in the case of seismic input EC8 and Tolmezzo, relatively high column RDD's were obtained. This is mainly due to the fact that in all cases the wall was designed only for the lower seismic input SIA.

The influence of the nonlinear behaviour of gravity load columns on the structural wall RDD was relatively small. As an average it produced a wall RDD reduction of about one. However, the variation due to different ground motions was more important.

The beneficial influence of the gravity load columns on the plastic hinge zone of the structural wall is mainly due to the energy dissipated by the nonlinear behaviour of the gravity load columns. The effect on the wall RDD is mainly seen for the EC8 and Tolmezzo earthquakes, for which the wall is rather underdesigned.

REFERENCES

Abaqus, Users' Manual, Hibbitt, Karlson, & Sorensen, Pawtucket, Rhode Island, 1991

Bachmann, H., Wenk, T., & Linde, P., Nonlinear Seismic Analysis of Hybrid Reinforced Concrete Frame Wall Buildings, Workshop on Nonlinear Seismic Analysis of R/C Buildings, July 13-16, 1992, Bled, Yugoslavia

Linde, P., Numerical Modelling of Structural Walls Subjected to Seismic Action, Swiss Federal Institute of Technology (ETH), Report in preparation

Paulay, T., & Priestley, M.J.N., Seismic Design of Reinforced Concrete and Masonry Buildings, John Wiley & Sons, New York, 1992

Paulay, T., Bachmann, H., & Moser, K., Erdbebenbemessung von Stahlbetonhochbauten, Birkhäuser Verlag, Basel-Boston, 1990

SIA Standard 160, Actions on Structures, Edition 1989 (in English), Swiss Society of Engineers and Architects, Zurich 1991

Wenk, T., Nichtlineare Berechnung von Stahlbetonrahmen unter Erdbebeneinwirkung, (in German) Swiss Federal Institute of Technology (ETH), Report in preparation